Supporting Information for "Reduced tropical climate land area under global warming"

Ori Adam[1], Noga Liberty-Levi[1], Michael Byrne[2,3], Thomas Birner[4]

[1]The Fredy and Nadine Herrmann Institute of Earth Sciences, The Hebrew University, Jerusalem, Israel

[2]School of Earth and Environmental Sciences, University of St Andrews, St Andrews, UK

[3]Department of Physics, University of Oxford, Oxford, UK

[4]Meteorologisches Institut, Ludwig-Maximilians-Universität, Munich, Germany

Supporting figures and tables

1. Figure S1: Daily climatologies of $\Delta_{Seasonal}$ and $\Delta_{Diurnal}$
2. Figure S2: $\Delta_{Seasonal}$ and $\Delta_{Diurnal}$ in CMIP5 and CMIP6 models
3. Figure S3: PDFs of end of 20th and end of 21st centuries
4. Figure S4: PDFs of regional changes in tropical land areas
5. Figure S5: Agreement across CMIP5/6 models by grid point
6. Table S1: CMIP5 and CMIP6 models' names and affiliations

Supporting information

a. Seasonal and diurnal temperature variations

The observed climatologies of surface temperature deviations from annual mean and of the diurnal surface temperature range are shown in Figure S1, zonally averaged over land. These variations are larger by factors of about 2 and 10 compared to the variations over oceans. However, the above factors can vary, as diurnal and seasonal land surface variations modulate adjacent ocean variations in some regions (Yang & Slingo, 2001).

If seasonal tropical temperature variations were determined solely by the seasonal march of peak insolation, temperatures near the equator would show two equinoctial peaks. The lack of a dominant semi-annual mode in temperature variations near the equator (Figure S1a) therefore indicates that additional processes, related to the dynamics of the tropical rain belt, are important (Riehl, 1954). The seasonal migrations of the tropical rain belt also affect diurnal temperature variations, which are smaller in heavily precipitating areas. Therefore, since we calculate $\Delta_{Diurnal}$ using annual means (derived from monthly means), we note that this definition fails to capture: (i) seasonal migrations of the equatorial minimum in $\Delta_{Diurnal}$, and (ii) increased $\Delta_{Diurnal}$ in subtropical latitudes ($\sim$20°) during winter.

b. Differences between CMIP5 and CMIP6 models

Figure S2 shows $\Delta_{Seasonal}$ and $\Delta_{Diurnal}$ in CMIP5 (pink) and CMIP6 (blue) models, averaged over land. The differences between the two CMIP phases the statistically insignificant in all tropical latitudes. We therefore analyze the two phases jointly.

c. Changes in tropical land area

Figure S3a,b compares end of 20th and end of 21st centuries' probability distribution functions (PDFs) of tropical land width (mean latitudinal extent of land where $\Delta_{Diurnal} > \Delta_{Seasonal}$) and of tropical land area (net land area where $\Delta_{Diurnal} > \Delta_{Seasonal}$), across the 45 CMIP5/6 models. A clear shift toward reduced tropical width and area is seen by the end of the 21st century, indicating a reduced net tropical extent under global warming (ensemble mean decrease in width and area is 2.9° and $3.1{\cdot}10^6$ km^2). Similar PDFs of the extent of the subtropical dry zones (SDZs), and of the width of the tropical rain belt (TRB), averaged globally and over land, are shown in Figure S3c-e.

Figure S4 shows regional PDFs of changes in tropical land area. Significant decrease is seen in the African and American sectors, whereas a negligible change is seen in the Asia–Western-Pacific sector. As an indication of the robustness of the projected changes, Figure S5a shows the sum over the sign of the change in $\Delta_{Diurnal} - \Delta_{Seasonal}$ across models, by grid point. The changes are most robust in the African and south American regions. Figure S5b-c shows similar sums due to the individual changes in $\Delta_{Seasonal}$ and $\Delta_{Diurnal}$ (i.e., holding $\Delta_{Diurnal}$ fixed in Figure S5b and holding $\Delta_{Seasonal}$ fixed in Figure S5c). The projected reduction in net tropical land area is thus primarily driven by increased $\Delta_{Seasonal}$ over Africa and the Americas, with some contribution by reduced $\Delta_{Diurnal}$ over northern Africa.

References

Bell, B., Hersbach, H., Simmons, A., Berrisford, P., Dahlgren, P., Horányi, A., ... others (2021). The era5 global reanalysis: Preliminary extension to 1950. *Quarterly Journal of the Royal Meteorological Society*, *147*(741), 4186–4227.

Hersbach, H., Bell, B., Berrisford, P., Hirahara, S., Horányi, A., Muñoz-Sabater, J., ... others (2020). The era5 global reanalysis. *Quarterly Journal of the Royal Meteorological Society*, *146*(730), 1999–2049.

Riehl, H. (1954). *Tropical meteorology* (Tech. Rep.). McGraw-Hill.

Yang, G.-Y., & Slingo, J. (2001). The diurnal cycle in the tropics. *Monthly Weather Review*, *129*(4), 784–801.

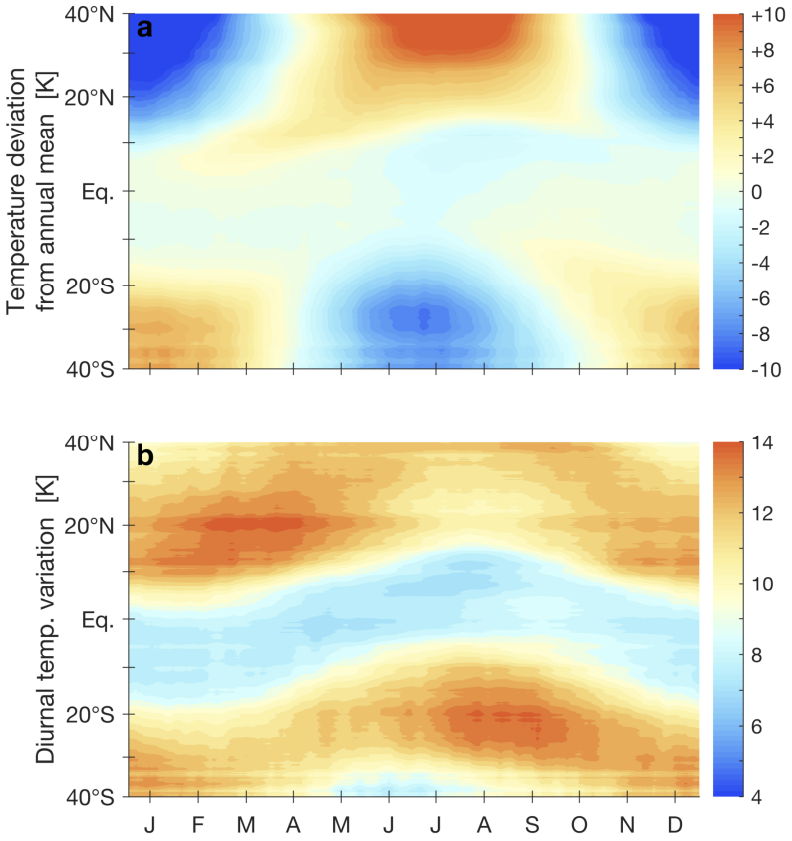

Figure S1. Daily climatologies of (**a**) surface temperature deviation from annual mean, and (**b**) diurnal surface temperature variations, zonally averaged over land areas. Data taken from ERA5 (Hersbach et al., 2020; Bell et al., 2021) for the years 1979–2019, smoothed with a 7-day centered running mean.

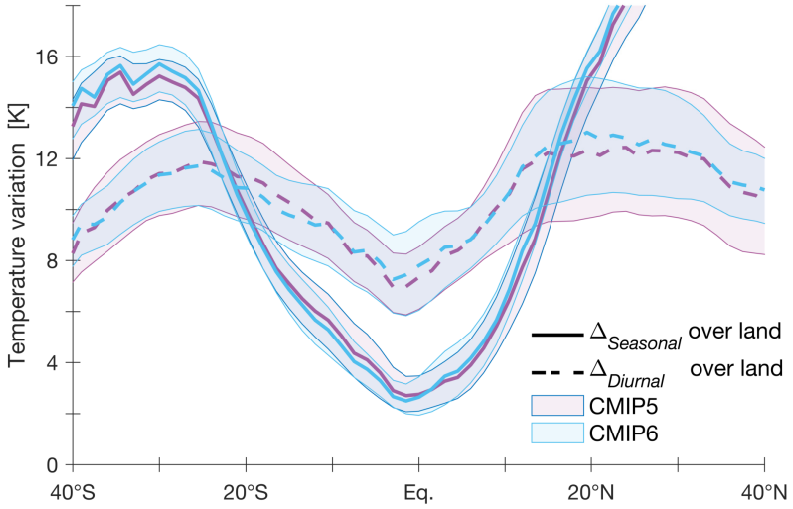

Figure S2. Amplitude of seasonal (solid) and diurnal (dashed) temperature variations ($\Delta_{Seasonal}$ and $\Delta_{Diurnal}$, respectively), zonally averaged over land areas, for CMIP5 (pink) and CMIP6 (blue) models. Bold lines show ensemble means; shading indicates ±1 standard deviation across models in each CMIP phase.

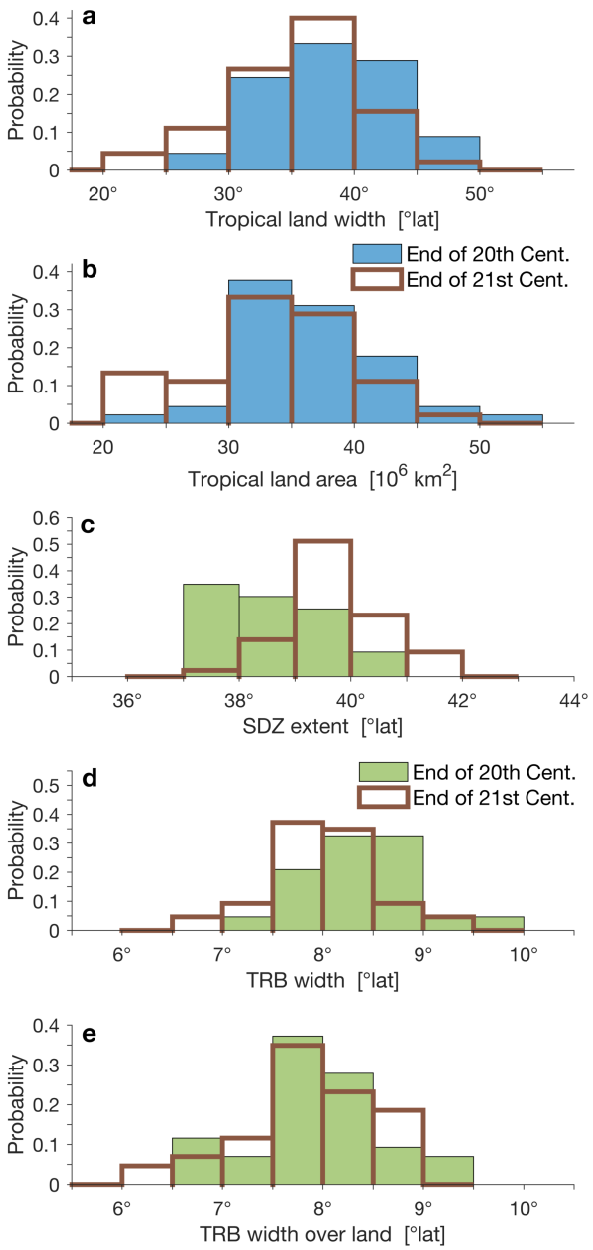

Figure S3. Probability distribution functions of (**a**) tropical land width (mean latitudinal extent of land where $\Delta_{Diurnal} > \Delta_{Seasonal}$), (**b**) tropical land area (net land area where $\Delta_{Diurnal} > \Delta_{Seasonal}$), (**c**) the extent of the subtropical dry zones (SDZs), (**d**) width of the tropical rain belt (TRB), and (**e**) width of the TRB over land. End of 20th century and end of 21st century values are shown in blue/green bars and brown lines, respectively. Note that the PDFs are composed of 45 models in panels a and b, and of 43 models in panels c–e.

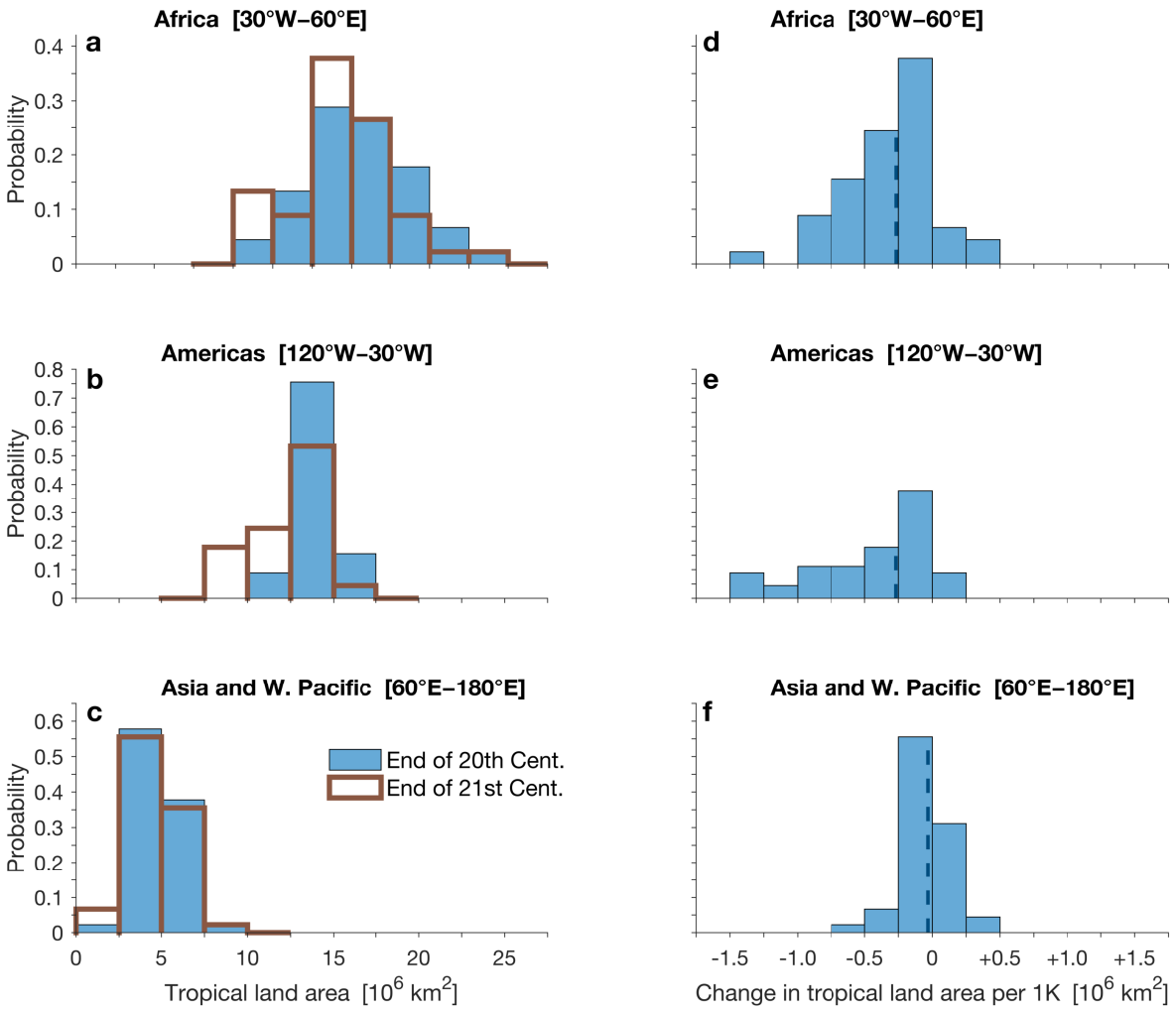

Figure S4. Left panels show the probability distribution functions (PDFs) of changes in tropical land area over the (**a**) African, (**b**) the Americas, and (**c**) Asia and western-Pacific sectors. Blue bars and brown lines indicate PDFs for the end of the 20th century (1980–1999) and end of 21st century (2080–2099), respectively. Right panels show PDFs of the corresponding changes, with vertical lines indicating medians.

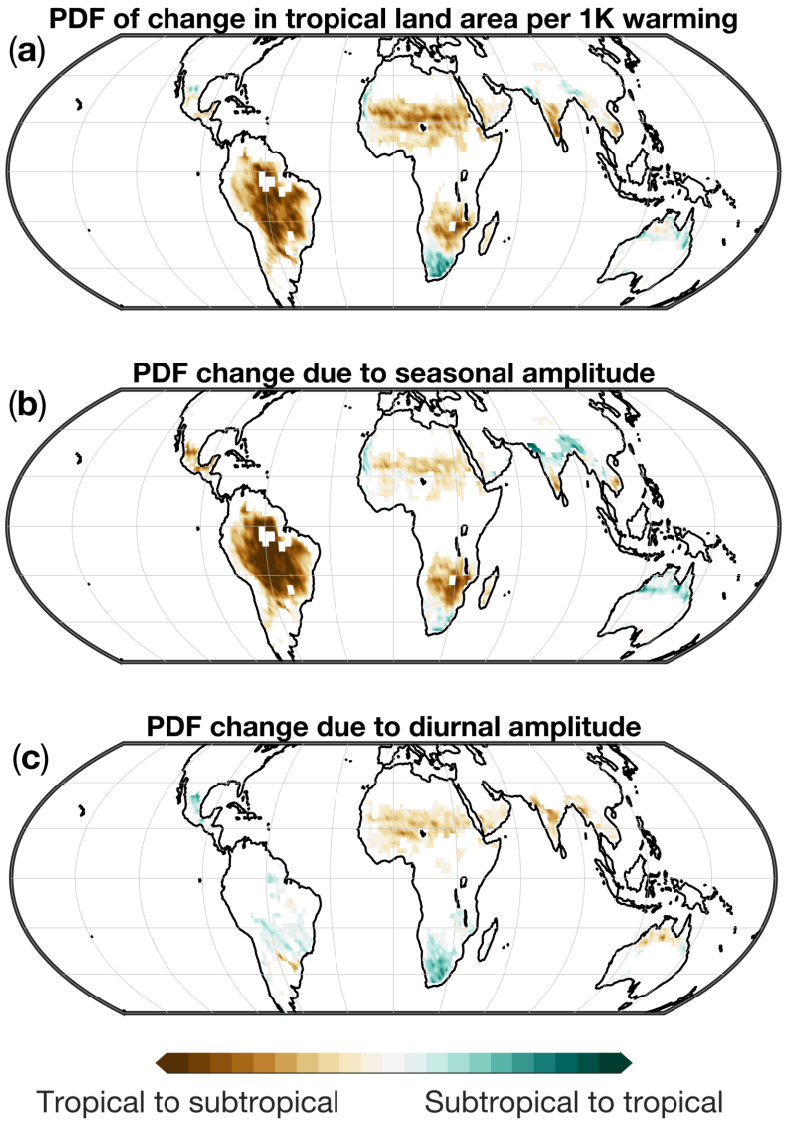

Figure S5. Sum over the sign of the change in $\Delta_{Diurnal} - \Delta_{Seasonal}$ across models by grid point, for (**a**) $\Delta_{Diurnal} - \Delta_{Seasonal}$, (**b**) changes due to $\Delta_{Seasonal}$ (i.e., $\Delta_{Diurnal}$ is held fixed), and (**c**) changes due to $\Delta_{Diurnal}$ (i.e., $\Delta_{Seasonal}$ is held fixed). Negative (brown) and positive (green) values indicate decrease and increase in tropical land area, respectively. White colors indicate equal number of models showing positive and negative changes in $\Delta_{Diurnal} - \Delta_{Seasonal}$.

Table S1. CMIP5 and CMIP6 models' names and affiliations. The two CMIP6 models for which precipitation minus evaporation is not available are marked with an asterisk.

Affiliation	**CMIP5 Model**	**CMIP6 Model**
CSIRO, and Bureau of Meteorology, Australia	ACCESS1-0	ACCESS-CM2
	ACCESS1-3	ACCESS-ESM1-5
	CSIRO-Mk3-6-0	
Beijing Climate Center (BCC), China		BCC-CSM2-MR
Chinese Academy of Science (CAS), China		CAS-ESM2-0*
Centro Euro-Mediterraneo sui Cambiamenti Climatici (CMCC), Italy	CMCC-CESM	CMCC-ESM2
	CMCC-CM	
	CMCC-CMS	
CCCma, Canada	CanESM2	CanESM5
CNRM and CERFACS, France	CNRM-CM5	
EC-Earth consortium		EC-Earth3
		EC-Earth3-veg
LASG/IAP, China		FGOALS-g3
FIO, QNLM, China		FIO-ESM-2-0
NOAA GFDL, USA	GFDL-CM3	GFDL-ESM4*
	GFDL-ESM2G	
	GFDL-ESM2M	
NASA / GISS, USA	GISS-E2-H	
	GISS-E2-H-CC	
	GISS-E2-R	
	GISS-E2-R-CC	
Met Office Hadley Centre, UK	HadGEM2-AO	
	HadGEM2-CC	
	HadGEM2-ES	
INM, Russia	inmcm4	INM-CM4-8
		INM-CM5-0
Institut Pierre Simon Laplace (IPSL), France		IPSL-CM6A-LR
JAMSTEC, AORI, and NIES, Japan	MIROC-ESM	MIROC6
	MIROC-ESM-CHEM	
	MIROC5	
Max Planck Institute for Meteorology (MPI), Germany	MPI-ESM-LR	MPI-ESM1-2-HR
	MPI-ESM-MR	MPI-ESM1-2-HR
Meteorological Research Institute (MRI), Japan	MRI-CGCM3	MRI-ESM2-0
	MRI-ESM1	
Norwegian Climate Centre, Norway	NorESM1-M	